Title

Short- and Long-Range Attractive Forces That Influence the Structure of Montmorillonite Osmotic Hydrates

Journal

Langmuir, 32(46)

ISSN

0743-7463

Authors

Tester, Chantel C
Aloni, Shaul
Gilbert, Benjamin
et al.

Publication Date

2016-11-22

DOI

10.1021/acs.langmuir.6b03265

Peer reviewed

Short- and Long-Range Attractive Forces That Influence the Structure of Montmorillonite Osmotic Hydrates

Chantel C. Tester†, Shaul Aloni‡, Benjamin Gilbert†, and Jillian F. Banfield†§

†Energy Geosciences Division and ‡Molecular Foundry, Lawrence Berkeley National Laboratory, Berkeley, California 94720, United States

§ Earth and Planetary Science, University of California, Berkeley, Berkeley, California 94720, United States

Publication Date (Web): November 10, 2016

DOI: 10.1021/acs.langmuir.6b03265

Abstract

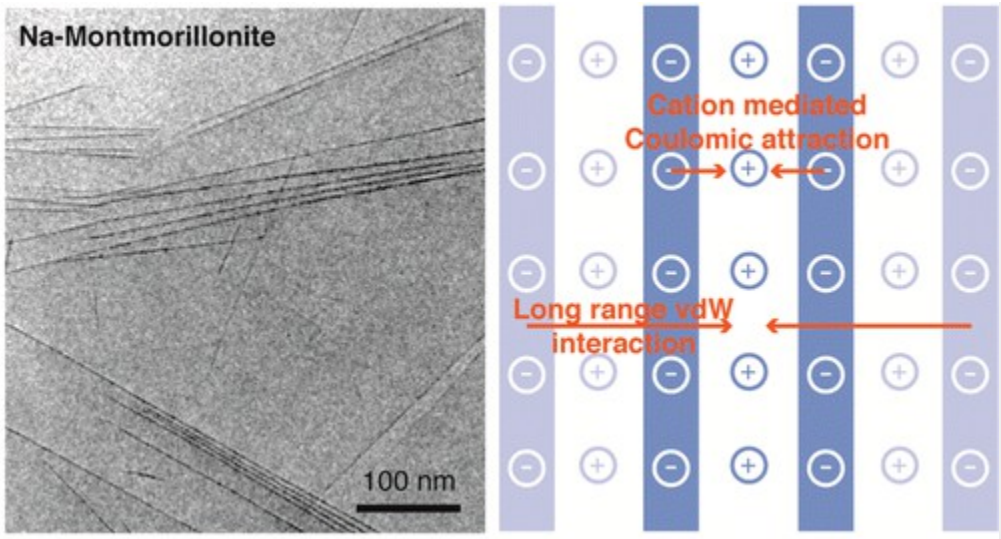

Clay swelling is a colloidal phenomenon that has a large influence on flow and solute migration in soils and sediments. While models for clay swelling have been proposed over many years, debate remains as to the interaction forces that combine to produce the observed swelling behavior. Using cryogenic transmission electron microscopy (cryo-TEM) and small-angle X-ray scattering, we study the influence of salinity, in combination with layer charge, interlayer cation, and particle size, on montmorillonite swelling. We observe a decrease in swelling with increased layer charge, increased cation charge, and decreased cation hydration, each indicative of the critical influence of Coulombic attraction between the negatively charged layers and interlayer cations. Cryo-TEM images of individual montmorillonite particles also reveal that swelling is dependent upon the number of layers in a particle. Calculations of the van der Waals (vdW) interaction based on new measurements of Hamaker coefficients confirm that long-range vdW interactions extend beyond near-neighbor layer interactions and result in a decrease in layer spacing with a larger number of layers. This work clarifies the short- and long-range attractive interactions that govern clay structure and ultimately the stability and permeability of hydrated clays in the environment.

Introduction

Clay swelling plays an essential role in many environmental and industrial processes, including the flow of water, hydrocarbons, and supercritical CO_2 in soils and sediments, and transport of radionuclides and other contaminants through clay barriers.(1) Swelling is commonly observed in smectites, a group of 2:1 layer silicates that, as a result of isomorphous substitutions in their octahedral or tetrahedral sheets, have a low negative layer charge that is compensated by exchangeable cations in the interlayer space.(2, 3) While clay swelling has been shown to be a function of several parameters, of particular interest is the influence of salinity.(4-6) Changes in the clay structure in response to changes in groundwater salinity can have a large influence on the stability and permeability of engineered clay barriers used in subsurface storage of nuclear waste and natural shale deposits selected as barriers for geologic storage of carbon dioxide.(7, 8)Salinization of soils as a result of irrigation or seawater intrusion similarly affects the ability of soils to absorb and retain water and other nutrients.

The general salinity dependence of smectite swelling behavior is well-established by X-ray diffraction (XRD) and small-angle X-ray scattering (SAXS).(4-6, 9) In a landmark study, Norrish and Quirk used XRD to measure the layer spacing of montmorillonite, a member of the smectite group, at varying concentrations of NaCl.(9) In highly saline aqueous solutions, e.g., 1 M NaCl, Wyoming montmorillonite exists as crystalline hydrates with a monolayer of interlayer water. Decreasing salinity leads to stepwise incorporation of two, three, and possibly four discrete layers of water. A discontinuous transition occurs at 0.25 M NaCl, with the layer spacing jumping from 2 to 4 nm. Below this salinity, the layer spacing increases continuously, with layer spacings as high at 28 nm reported.(6) In this regime, the swelling is described as osmotic swelling because it is driven by the difference in ion concentrations inside and outside of the clay layers. At still lower salinities, further expansion eventually results in complete delamination of the montmorillonite particles into single layers.

Substantial research has generated structural models and theoretical descriptions of smectite crystalline hydrates and fully exfoliated dispersions. For example, *c*-axis electron density profiles have been established to high accuracy for crystalline hydrates.(10) Clear conceptual models exist for the dependence of crystalline hydrate layer spacing upon water activity, salinity, and layer charge, and molecular simulation can provide good agreement with swelling observations.(2, 11-13) Moreover, the structure and rheology of low-salinity suspensions of delaminated montmorillonite layers, including a transition between a completely dispersed sol and an aggregated gel, are well-established.(14, 15) In contrast, osmotic hydrates represent an intermediate regime for which a clear understanding of layer–layer interactions is lacking.

Clay swelling is governed by competing short- and long-range forces. These interactions are typically modeled by the theory of Derjaguin–Landau–Verwey–Overbeek (DLVO). The DLVO theory describes the interactions between two colloidal particles as a balance between electrostatic repulsion, in this case between two negatively charged clay layers, and vdW attraction. This theory accurately predicts the swelling behavior of smectites with low layer charge in the presence of monovalent Li^+ and Na^+.(16, 17) However, the DLVO theory fails to adequately describe the behavior of smectites with high layer charge or in the presence of divalent cations.(18-20) Beginning with Langmuir, the postulates of the DLVO theory have been criticized in part because of skepticism that vdW forces could act over the distances relevant to colloidal suspensions and osmotic hydrates.(21) As an alternative, Langmuir and later the Sogami–Ise theory proposed that long-range electrostatic attractive forces between like-charged particles could be mediated by intervening counterions.(22) This concept has experimental and theoretical support, but disagreement continues over the most appropriate description of clay swelling.(20) Layer–layer

interactions in smectites are further complicated by the presence of both negatively charged faces and positively charged edges.(23) This inhomogeneous charge distribution could influence the layer–layer equilibrium structure.

Direct determination of the forces between interfaces in water is feasible for only a minority of systems.(24) However, detailed knowledge of the structure of colloidal suspensions and the dependence of this structure upon particle and solution properties can provide insights into the nature of such interaction forces. Light, X-ray, and neutron scattering methods cannot fully describe complex anisotropic systems, such as smectite osmotic hydrates, but can provide statistically significant constraints upon models of the suspension structure. Here, we show that *in situ* imaging using cryo-TEM clarifies the attractive interaction forces that govern clay swelling.

Cryo-TEM of frozen hydrated clays provides unprecedentedly clear images of individual montmorillonite particles as they exist in solution.(25) In combination, SAXS provides complementary bulk characterization of the particle shape and layer spacing from the crystalline to osmotic hydrate regime. We used these methods to characterize the structure of hydrated montmorillonite as a function of salinity, in combination with layer charge, interlayer cation, and particle size. This work provides support for counterion-mediated attraction between negatively charged smectite layers within osmotic hydrates. In addition, our imaging results strongly indicate a role for long-range non-electrostatic attractive forces in influencing layer spacing. To confirm this conclusion, we used valence electron energy-loss spectroscopy (VEELS) and the Lifshitz theory to predict the contributions of vdW interactions to montmorillonite swelling. This work demonstrates the importance of long-range vdW forces to the structure of osmotic hydrates, thereby providing direct support for a key precept of the DLVO approach.

Experimental Section

Materials

Experiments were performed using Wyoming montmorillonite (SWy-2), Cheto montmorillonite (SAz-2), and Otay montmorillonite (SCa-3) from the Source Clays Repository of The Clay Minerals Society. The layer charges per unit formula are −0.55 (octahedral, −0.53; tetrahedral, −0.2), −1.08 (octahedral, −1.08; tetrahedral, 0), and −1.48 (octahedral, −1.29; tetrahedral, −0.19) for SWy-2, SAz-2, and SCa-3, respectively.(26) Aqueous solutions of NaCl, LiCl, KCl, $MgCl_2$, and $CaCl_2$ were prepared from reagent-grade salts and Milli-Q ultrapure water.

Clay Treatments

The clays were treated to obtain homoionic montmorillonite free of mineral impurities. This was achieved by equilibrating the clay (40 g/L) in 1 M NaCl solution. The supernatant was separated by centrifugation and replaced three times. Excess NaCl was removed by replacing the supernatant with ultrapure water, followed by dialysis [SpectraPor 7, 8 kDa molecular weight cut-off (MWCO), 40 mm flat width]. Large impurities (>2 μm), such as quartz or feldspar, were removed by centrifugation following the conditions described by Moore and Reynolds.(27)Additional size fractionation of the clay suspension was achieved by increasing the centrifugation time and speed. Exchange of interlayer Na^+ cations with Li^+, K^+, Mg^{2+}, or Ca^{2+} was achieved by repeating the equilibration in the respective chloride salts and removal of the excess salt. The clay suspensions were then

dried at 60 °C in a convection oven. Clays were rehydrated with water or aqueous salt solutions at 5 wt % and allowed to equilibrate for 1 week prior to characterization.

Cryo-TEM Sample Preparation and Imaging

Clay suspensions were plunge-frozen in liquid ethane using an automated vitrification robot (FEI Vitrobot). Aliquots of 3 μL were deposited onto 300-mesh lacy carbon Cu grids (Electron Microscopy Sciences) that had been glow-discharged. Excess solution was removed by automatic blotting (2 blots for 5 s each) before plunge freezing. Imaging was performed at 200 kV on a field-emission-gun-equipped Philips CM200. Vitrified samples were loaded using a Gatan cryo-holder operating at approximately −180 °C. Measurements of interlayer spacing were performed using the software ImageJ. Measurements were restricted to particles containing at least four layers and layers that appeared parallel or approximately parallel. The measurements were averaged within and, unless otherwise noted, across multiple particles to produce the reported interlayer spacings.

SAXS Data Collection

SAXS was performed at beamline 5-ID-D of the Advanced Photon Source at Argonne National Laboratory. Equilibrated clay suspensions were mounted in a 1.5 mm quartz capillary (Charles Supper Company). SAXS data were collected simultaneously on two Rayonix charge-coupled device (CCD) detectors with sample–detector distances of 8.5 and 1.0 m, calibrated using a lanthanum hexaborate and silver behenate standard, respectively. The wavelength of radiation was set to 1.03 Å (12 keV), resulting in a range of the scattering vector, q = 0.017–0.58 $Å^{-1}$. The scattering patterns were azimuthally averaged using FIT2D and corrected for varying incident beam intensity and sample transmission. The scattering intensity, $I(q)$, of the clay suspensions was obtained by subtracting contributions from the solution and the quartz capillary.

VEELS Data Collection and vdW Force Calculations

Hamaker coefficients for montmorillonite layers separated by water were calculated from measured VEELS–transmission electron microscopy (TEM) data following the method developed by the French group.(28) A suspension of Na-saturated SWy-2 in water was deposited on a lacy carbon TEM grid and allowed to dry. VEELS–TEM data were recorded on a 2100-F field-emission transmission electron microscope (FETEM) operating at 80 kV and processed using DigitalMicrograph software (Gatan). Two spectra, zero loss and plasmon peak optimized, were recorded and spliced, yielding a total energy range from −5 to 65 eV. The energy resolution based on the full width at half maximum of the zero-loss peak was 0.9 eV. To confirm that the sample was not significantly damaged as a result of irradiation by the electron beam, a microdiffraction pattern was recorded following VEELS–TEM data collection to confirm characteristic crystal diffraction. The zero-loss peak was removed from the VEELS–TEM spectra by fitting with a logarithmic tail, and multiple scattering was removed on the basis of the Fourier-log deconvolution method.(29) The imaginary component of the dielectric function was extracted by Kramers–Kronig analysis of the deconvolved spectra. The spectra were scaled according to the index of refraction sum rule scaling, assuming a refractive index perpendicular to the plane of the SWy-2 flake of n_α = 1.520 ± 0.003.(30) The Hamaker coefficient of SWy-2 separated by water (A) was calculated according to the Lifshitz theory,(31) implemented using the Gecko Hamaker code.(32)Calculations were performed assuming particles containing 2–16 montmorillonite layers of 1 nm thickness. The Hamaker coefficients were then used to calculate the vdW force per unit area, P_{vdW}, between two SWy-2 layers

$$P_{vdW} = \frac{A}{6\pi D^3}$$

where D is the layer spacing. Additional details of the VEELS–TEM analysis and Hamaker coefficient calculations are given in the Supporting Information.

Results and Discussion

Influence of Salinity

Cryo-TEM images of SWy-2 equilibrated at 0.01, 0.1, and 1 M NaCl demonstrate an increase in layer spacing with decreasing salinity (panels a–c of Figure 1). At 0.1 and 0.01 M NaCl, we observe both individual delaminated layers and osmotic hydrate particles containing multiple expanded layers. In these images, only clay particles with layers oriented parallel to the optical axis are visible. Clay particles in other orientations may be present, but because each layer is only approximately 1 nm thick, there is insufficient mass-thickness contrast to detect particles containing a small number of layers oriented more than 10° from the optical axis.(25)Measurements of the layer spacing both within a single particle and across multiple particles find a large variation in spacing. The average layer spacings at 0.1 and 0.01 M NaCl are 8 ± 1 and 11 ± 1 nm, respectively, both characteristic of osmotic swelling. At 1 M NaCl, we observe clay particles containing multiple stacked layers and a well-defined layer spacing of 1.9 ± 0.15 nm, characteristic of crystalline hydrates.

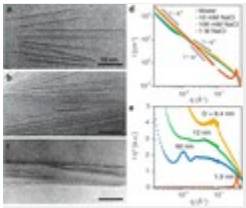

Figure 1. (a–c) Cryo-TEM images show the arrangement of 2:1 layers of SWy-2 imaged in cross section (dark lines) in (a) 0.01 M, (b) 0.1 M, and (c) 1 M NaCl solutions and reveal the morphology of smectite particles and disorder in layer spacing. (d and e) SAXS data from equivalent samples provide bulk characterization of the (d) particle shape from the power law slope [$I(q) \sim q^{-m}$] and (e) layer or particle spacing.

Within the range of salinities studied and in circumneutral and acidic solutions (pH 4), we observe predominantly face-to-face interactions. In agreement with indirect studies of the solution structure of other platelets, we find no evidence of the edge-to-face “house of cards” configuration that is thought to arise from protonation of clay particle edges. Some individual layers within osmotic hydrates exhibit layer rotations and lateral offsets that are suggestive of increased edge-to-face proximity, possibly a rotationally disordered version of the “stack of coins” configuration. However, a further study of SWy-2 equilibrated at pH 4 in 0.1 M NaCl did not show more examples, even though a more positive edge charge was expected.(23) Thus, we cannot confidently attribute the observed structure to random Brownian motion or electrostatic edge-to-face forces.

SAXS data of Na-saturated SWy-2 suspensions in 0–1 M NaCl provide complementary characterization of the smectite dispersions at several length scales. At low q, the scattering slope is $I(q) \sim q^{-3}$, characteristic of scattering from a mass fractal or three-dimensional particle. This suggests that, even at low salinity, the clay layers form large assemblies that do not completely

delaminate [also seen by Pignon and Ganley and van Duijneveldt using small-angle neutron scanning (SANS)/static light scattering (SLS)].(33, 34) At intermediate q ($0.01 < q < 0.05$), the power law slope for SWy-2 suspended in water or 0.1 M NaCl is $I(q) \sim q^{-2}$, characteristic of scattering from two-dimensional particles or sheets.

The SAXS data also exhibit broad peaks that demonstrate the transition from crystalline to osmotic swelling with decreasing salinity. Smectite in water gives the strongest SAXS peak at a 60 nm distance that is consistent with prior results on more concentrated suspensions.(6, 35, 36) In particular, Svensson and Henson also found a more pronounced scattering peak in water relative to NaCl solutions. SAXS data from smectite in pure water is quite accurately reproduced as repulsive interactions between disc-shaped particles with limited ordered stacking.(37) This is consistent with our cryo-TEM data that could not provide a statistically relevant assessment of interlayer spacing. Thus, the SAXS peak likely derives from a combination of scattering from disordered periodic lamellae and a suppression of scattering intensity as a result of repulsive layer–layer correlations.(33)

For SWy-2 suspended in 0.1 and 0.01 M NaCl, the SAXS peaks indicate disordered layer spacings of approximately 8.4 and 12 nm, respectively. These spacings are in good agreement with our cryo-TEM observations of disordered osmotic hydrates. At 1 M NaCl, the power law slope at intermediate q increases to $I(q) \sim q^{-3}$, consistent with the formation of aggregated crystalline hydrates. The well-defined peak corresponds to a crystalline layer spacing of 1.9 nm. The dependence of the crystalline and osmotic hydrate structures with ionic strength is in good agreement with DLVO.

Influence of the Layer Charge

To better understand the influence of layer charge, we also studied montmorillonites that have a higher layer charge than SWy-2 (−0.57 e^-/formula unit) as a result of substitutions in both their octahedral and tetrahedral sheets. Cryo-TEM images of SCa-3 (−1.48 e^-/formula unit) and SAz-2 (−1.08 e^-/formula unit) equilibrated in 0.01 M NaCl show osmotic hydrates with lower average layer spacings of 7 ± 1 and 6.5 ± 0.9 nm, respectively (Figure 2). SCa-3 and SAz-2 form aggregates containing a larger number of layers with more disorder than observed in SWy-2 suspensions. SAXS data of SCa-3 and SAz-2 suspensions indicate the coexistence of two distinct layer spacings of 6.5 nm, also observed by cryo-TEM, and 1.9 nm, characteristic of crystalline hydrates. The ratio of the intensities of the osmotic and crystalline hydrate peaks increases with decreasing layer charge.

Figure 2. (a and b) Cryo-TEM images of (a) SCa-3 and (b) SAz-2 in 0.01 M NaCl, which have approximately 2 and 3 times the layer charge of SWy-2, respectively. (c) SAXS data reveal two distinct layer spacings corresponding to osmotic and crystalline hydrates. The position of the osmotic and crystalline hydrate peaks are similar in the SCa-3 and SAz-2 suspensions, but the ratio of their intensities increases with decreasing layer charge.

A relationship between layer charge and swelling of crystalline hydrates has been previously established. Slade and co-workers observed that higher charge smectites either did not expand or required lower salt concentrations to transition from the one- to two-layer hydrate.(38) Dazas and co-workers observed a decrease in smectite crystalline layer spacing with charge of the tetrahedral sheet.(10) In contrast, there is no consistent picture of layer charge and swelling in the osmotic hydrate regime.(2) Reports of swelling pressure have provided either very small or undetectable dependence upon layer charge, but those

measurements cannot distinguish layer and smectite particle contributions to the swelling pressure.(39, 40) Thus, the present work is the first demonstration of an influence of layer charge on the mean layer spacing of osmotic hydrates, a relationship that is not reproduced by the DLVO theory.(2) Although a full model of swelling is out of the scope of this paper, it is a clear demonstration of attractive electrostatic forces within the smectite layers and the interlayer cations.

Effect of the Cation Type

We further investigate the influence of Coulombic attraction between clay layers and interlayer cations by studying the effect of exchanging the interlayer cations. SWy-2, which predominantly contains interlayer Na^+ cations, was exchanged with monovalent Li^+ and K^+ cations and divalent Mg^{2+} and Ca^{2+} cations by equilibrating the clay with the respective chloride salts. In SWy-2 exchanged with Li^+ and rehydrated at 0.1 M LiCl, we observe osmotic hydrates with morphologies and layer spacings that are similar to those observed with Na-saturated SWy-2 at an equal salt concentration (Figure 3a). The layer spacings are also in agreement with observations by Norrish using XRD.(5) In contrast, exchange of the interlayer cations with either Mg^{2+} or Ca^{2+} resulted in a highly ordered layer spacing of 2 ± 0.1 nm, characteristic of crystalline hydrates (panels c and d of Figure 3 and Figure S1 of the Supporting Information). Multivalent cations have long been known to inhibit clay swelling and prevent the formation of osmotic hydrates, even at very low ionic strength.(5) Similar to the effect of layer charge, the decrease in layer spacing with cation charge is attributed to an increase in the Coulombic attraction between the clay layers and the interlayer divalent cations.

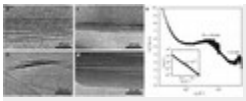

Figure 3. (a–d) Cryo-TEM images of (a) Li-, (b) K-, (c) Mg-, and (d) Ca-saturated SWy-2 in 0.1 M corresponding chloride salt solutions. (e) SAXS data of K-saturated SWy-2 in 0.1 M KCl displays two distinct layer spacings at high q (D = 1.5 nm) and low q (D = 13 nm).

We also chose to investigate the effect of K^+ because this monovalent cation is known to interact distinctively with swelling clays.(41-44) High concentrations of KCl are used in water-based drilling fluids to prevent clay swelling and wellbore instability during oil and gas exploration.(45) Inhibition of clay swelling is typically attributed to the low hydration energy of K^+ and ability to form inner-sphere surface complexes with the smectite basal surface.(41, 42) Using XRD, Berend and Ferrage found that, at high relative humidity, montmorillonite exchanged with cations with higher hydration energies, such as Li^+, Na^+, Mg^{2+}, and Ca^{2+}, predominantly contains two water layers, whereas montmorillonite exchanged with cations with lower hydration energies, such a K^+, contains zero and/or one water layer.(46, 47) Molecular simulations further confirm that the single-layer hydrate with K^+ ions bound to the clay surface is the most energetically stable structure for K-saturated montmorillonite.(43)

Cryo-TEM revealed both unexpanded clay particles and delaminated clay layers but no evidence of osmotic hydrates (Figure 3b). No other cation generated this combination. SAXS of K-saturated SWy-2 suspensions exhibited a peak at 1.4 nm, confirming the presence of unexpanded clay layers (Figure 3e). The power slope of $I(q) \sim q^{-2.3}$ also supports the presence of expanded and aggregated clay layers. Unexpectedly, on the basis of the highly disordered suspensions observed with cryo-TEM, the SAXS data also showed a broad second peak at 13 nm, characteristic of osmotic hydrates. These SAXS observations are in agreement with prior work. In XRD studies of >33 wt % K-saturated Upton montmorillonite in water, Zhang and Low

report the presence of two peaks corresponding to crystalline (∼1.5 nm) and osmotic (5.5–8.5 nm) hydrates.(44) These data at high clay content are consistent with our own, because it is well-established that osmotic layer spacing increases at a lower clay content. The presence of smectite in all swelling states in a single suspension is surprising. More work will be required to understand K^+ interactions with smectite and the poor agreement with SAXS and cryo-TEM for this system.

Influence of the Layer Dimension

We hypothesized that the significant disorder observed in the smectite suspensions may be a consequence of a broad distribution of smectite layer sizes. Na-saturated SWy-2 was size-fractionated in water by centrifugation, and the fractions resuspended in 0.1 M NaCl. Cryo-TEM and SAXS (Figure 4) showed that the resulting fractions were distinct but provided little evidence for size fractionation based on the layer diameter. Cryo-TEM images of the large size fraction display aggregates composed of many layers and layer spacings characteristic of both osmotic and crystalline hydrates. This is also reflected in the SAXS data from the presence of two peaks corresponding to layer spacings of 7.3 and 1.9 nm (Figure 4d). In the smallest size fraction, we observe by cryo-TEM only single delaminated clay layers and minimal evidence of osmotic hydrates. In SAXS, this is reflected from the power log slope of $I(q) \sim q^{-2}$, even at low q (Figure 4c). Segad and co-workers also investigated the influence of size fractionation and report based on Scherrer analysis of SAXS peak widths that the number of layers in the particle increases in larger size fractions.(35) No evidence of ordered layer stacking was observed in the smallest size fraction.

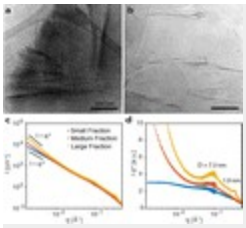

Figure 4. (a and b) Cryo-TEM images of Na-saturated SWy-2 fractionated in water and then suspended in 0.1 M NaCl. (a) The large size fraction contains primarily large aggregates, while (b) the small size fraction contains single delaminated clay layers. (c and d) Corresponding SAXS data of the small, medium, and large size fractions.

Together these observations suggest that there is a fraction of clay layers in Na-saturated SWy-2 that does not completely delaminate, even in water, and a fraction that does not reassemble into stacked layers, even at salinities as high as 0.1 M NaCl. This is also supported by SAXS data of Na-saturated SWy-2 in water, which indicates the presence of large clay assemblies, even at very low salinity (Figure 1d). The centrifugation method, therefore, did not fractionate based on the diameter of the clay layers, instead fractionating based on the particle size (number of stacked layers). We suggest that this finding is a result of the inherent composition and charge heterogeneity of natural clays. The largest size fraction may have a higher layer charge that inhibits delamination or exchange with Na^+, while the smallest size fraction may have a lower layer charge and, consequently, minimal Coulombic attraction between the clay layers and interlayer cations.

Relationship between the Layer Number and Interlayer Spacing

Cryo-TEM imaging of individual clay particles also allows us to correlate the measured interlayer spacings with the observed number of layers in a particle. Despite large variation in the measured layer spacings, even within a single particle, we observe a decrease in spacing with an increasing number of clay layers (panels a–c of Figure 5). For SWy-2 suspended in 0.1 M NaCl, the majority of particles contain 4 or 5 layers; however, particles with as high as 15 layers are observed. Measurements of the

average layer spacing within a single particle indicate a decrease in layer spacing from 8.2 nm in particles containing 4 layers to 6.3 nm in particles containing 15 layers. As proposed in earlier work, we attribute this decrease in layer spacing with a larger number of layers to the influence of long-range vdW interactions, with long-range defined here as those extending beyond near-neighbor layer interactions.(25) Although electrostatic interactions between smectite layers and electrolyte cations can cause pairwise attractive forces between smectite layers, no theory of colloidal interactions has shown how electrostatic forces could extend over multiple layers.

Figure 5. (a–c) Cryo-TEM images of Na-saturated SWy-2 in 0.1 M NaCl demonstrate a decrease in layer spacing with an increasing number of layers (N_{layers}) from (a) 4 to (b) 15. (d) P_{vdW} as a function of N_{layers} at fixed layer spacing (D = 8 nm) and variable layer spacings taken from cryo-TEM measurements at 0.1 M NaCl (D = 8–6 nm).

Accurate models of the vdW forces between clay layers depend upon accurate values of the Hamaker coefficient.(24) These values can be calculated from optical absorption measurements, but as a result of the nanoscale dimensions of smectite particles, published Hamaker coefficients are based on indirect measurements and exhibit considerable variation.(48, 49) To obtain reliable values of the Hamaker coefficient, we use VEELS–TEM to measure the optical absorption of individual Na-saturated SWy-2 layers (Figure S2 of the Supporting Information). From measured spectra, we can extract the dielectric function and apply the Lifshitz theory to calculate values of the Hamaker coefficient as a function of the number of layers in a particle and their separation. For two SWy-2 layers of finite thickness, we obtain a non-retarded Hamaker coefficient of 8 ± 1 zJ (Figure S3 of the Supporting Information). This value is in good agreement with a model constructed from silica and corundum optical data(25) but is lower than values that have been obtained on the basis of swelling pressure (18.8–64.9 zJ) or critical coagulation concentration (22 zJ).(48, 49)

From the measured values of the Hamaker coefficient, we can calculate P_{vdW} between two SWy-2 layers as a function of the number of layers in the particle (Figure 5d). Assuming a fixed layer spacing (D = 8 nm, the value for a particle containing two layers extrapolated from cryo-TEM data of SWy-2 in 0.1 M NaCl), we estimate that P_{vdW} increases slowly from 16 N m^{-2} for a particle containing two layers to 20 N m^{-2} for a particle containing 16 layers. If we also account for the decrease in layer spacing observed by cryo-TEM, P_{vdW} between two SWy-2 layers increases exponentially, with the addition of each successive layer. For SWy-2 at 0.1 M NaCl, we estimate that P_{vdW} between two layers increases from 16 to 60 N m^{-2} in a particle containing 16 layers. This relationship between the particle size and layer spacing arising from long-range vdW interactions thus predicts the inverse relationship between the layer spacing and particle size that we observe by cryo-TEM.(25) Our experimental observations and quantitative vdW force calculations, as well as the recent advances in understanding vdW forces in a range of systems,(50, 51) clearly establish long-range vdW forces to be a central aspect of clay swelling as originally proposed by the developers of the DLVO theory.

Conclusion

Using cryo-TEM and SAXS, we characterize the structure of montmorillonite suspensions as a function of salinity, in combination with the layer charge, interlayer cation, and particle size. The observations show an important role for short-range attractive Coulombic interactions between negatively charged smectite layers and interlayer cations that oppose swelling in both the crystalline and osmotic hydrate regimes. In the osmotic swelling regime, we find evidence for long-range vdW attraction that contributes to ordered layer spacings, even out to large separations across multiple smectite layers. These findings confirm the role of vdW forces as described by the DLVO theory but clarify the need to consider multilayer interactions for a full description of clay swelling. The combination of *in situ* characterization and measurement of vdW interactions by VEELS–TEM provides a basis for identifying and modeling the relevant interaction forces that control swelling in natural clay systems.

Supporting Information

The authors declare no competing financial interest.

Acknowledgment

The authors thank Roseann Csencsits and Zoltan Metlagel for their help with cryo-TEM. This work was supported by the Office of Science, Office of Basic Energy Sciences (BES), Chemical Sciences, Geosciences, and Biosciences Division of the U.S. Department of Energy (DOE), under Contract DE-AC02-05CH11231. Research at the Molecular Foundry was supported by BES, DOE, under Contract DE-AC02-05CH11231.

References

This article references 51 other publications.

1. *Handbook of Clay Science*; Biergaya, F., Lagaly, G., Eds.; Elsevier: Amsterdam, Netherlands, **2013**.

2. Laird, D. A. Influence of layer charge on swelling of smectites *Appl. Clay Sci.* **2006**, 34, 74– 87 DOI: 10.1016/j.clay.2006.01.009

3. Low, P. F.; Margheim, J. F. The Swelling of Clay: I. Basic Concepts and Empirical Equations *Soil Sci. Soc. Am. J.* **1979**, 43, 473– 481 DOI: 10.2136/sssaj1979.03615995004300030010x

4. Amorim, C.; Lopes, R.; Barroso, R.; Queiroz, J.; Alves, D.; Perez, C.; Schelin, H. Effect of clay–water interactions on clay swelling by X-ray diffraction *Nucl. Instrum. Methods Phys. Res., Sect. A* **2007**, 580,768– 770 DOI: 10.1016/j.nima.2007.05.103

5. Norrish, K. The swelling of montmorillonite *Discuss. Faraday Soc.* **1954**, 18, 120– 134 DOI: 10.1039/df9541800120

6. Svensson, P. D.; Hansen, S. Combined Salt and Temperature Impact on Montmorillonite Hydration *Clays Clay Miner.* **2013**, 61, 328– 341 DOI: 10.1346/CCMN.2013.0610412

7. Busch, A.; Alles, S.; Gensterblum, Y.; Prinz, D.; Dewhurst, D. N.; Raven, M. D.; Stanjek, H.; Krooss, B. M.Carbon dioxide storage potential of shales *Int. J. Greenhouse Gas Control* **2008**, 2, 297– 308 DOI: 10.1016/j.ijggc.2008.03.003

8. Nowak, E. J. The Backfill as an Engineered Barrier for Nuclear Waste Management. In *Scientific Basis for Nuclear Waste Management*; Northrup, C. J. M., Jr., Ed.; Springer: New York, **1980**; pp 403– 411.

9. Norrish, K.; Quirk, J. P. Crystalline Swelling of Montmorillonite: Use of Electrolytes to Control Swelling*Nature* **1954**, 173, 255– 256 DOI: 10.1038/173255a0

10. Dazas, B.; Lanson, B.; Delville, A.; Robert, J.-L.; Komarneni, S.; Michot, L. J.; Ferrage, E. Influence of Tetrahedral Layer Charge on the Organization of Interlayer Water and Ions in Synthetic Na-Saturated Smectites *J. Phys. Chem. C* **2015**, 119, 4158– 4172 DOI: 10.1021/jp5123322

11. Kleijn, W. B.; Oster, J. D. A model of clay swelling and tactoid formation *Clays Clay Miner.* **1982**, 30, 383–390 DOI: 10.1346/CCMN.1982.0300509

12. Hensen, E. J. M.; Smit, B. Why clays swell *J. Phys. Chem. B* **2002**, 106, 12664– 12667 DOI: 10.1021/jp0264883

13. Whitley, H. D.; Smith, D. E. Free energy, energy, and entropy of swelling in Cs–, Na–, and Sr–montmorillonite clays *J. Chem. Phys.* **2004**, 120, 5387– 5395 DOI: 10.1063/1.1648013

14. Michot, L. J.; Bihannic, I.; Porsch, K.; Maddi, S.; Baravian, C.; Mougel, J.; Levitz, P. Phase Diagrams of Wyoming Na-Montmorillonite Clay. Influence of Particle Anisotropy *Langmuir* **2004**, 20, 10829– 10837 DOI: 10.1021/la0489108

15. Paineau, E.; Michot, L. J.; Bihannic, I.; Baravian, C. Aqueous Suspensions of Natural Swelling Clay Minerals. 2. Rheological Characterization *Langmuir* **2011**, 27, 7806– 7819 DOI: 10.1021/la2001267

16. Quirk, J.; Marcelja, S. Application of double-layer theories to the extensive crystalline swelling of Li-montmorillonite *Langmuir* **1997**, 13, 6241– 6248 DOI: 10.1021/la970484l

17. Greathouse, J. A.; Feller, S. E.; McQuarrie, D. A. The Modified Gouy-Chapman Theory: Comparisons between Electrical Double Layer Models of Clay Swelling *Langmuir* **1994**, 10, 2125– 2130 DOI: 10.1021/la00019a018

18. Jellander, R.; Marčelja, S.; Quirk, J. Attractive double-layer interactions between calcium clay particles *J. Colloid Interface Sci.* **1988**, 126, 194– 211 DOI: 10.1016/0021-9797(88)90113-0

19. McBride, M.; Baveye, P. Diffuse Double-Layer Models, Long-Range Forces, and Ordering in Clay Colloids*Soil Sci. Soc. Am. J.* **2002**, 66, 1207– 1217 DOI: 10.2136/sssaj2002.1207

20. McBride, M. B. A critique of diffuse double layer models applied to colloid and surface chemistry *Clays Clay Miner.* **1997**, 45, 598– 608 DOI: 10.1346/CCMN.1997.0450412

21. Langmuir, I. The role of attractive and repulsive forces in the formation of tactoids, thixotropic gels, protein crystals and coacervates *J. Chem. Phys.* **1938**, 6, 873– 896 DOI: 10.1063/1.1750183

22. Ise, N. Like likes like: Counterion-mediated attraction in macroionic and colloidal interaction *Phys. Chem. Chem. Phys.* **2010**, 12, 10279– 10287 DOI: 10.1039/c000729c

23. Tournassat, C.; Ferrage, E.; Poinsignon, C.; Charlet, L. The titration of clay minerals: II. Structure-based model and implications for clay reactivity *J. Colloid Interface Sci.* **2004**, 273, 234 DOI: 10.1016/j.jcis.2003.11.022

24. Israelachvili, J. N. *Intermolecular and Surface Forces*, 3rd ed.; Academic Press: Waltham, MA, **2011**.

25. Gilbert, B.; Comolli, L. R.; Tinnacher, R. M.; Kunz, M.; Banfield, J. F. Formation and Restacking of Disordered Smectite Osmotic Hydrates *Clays Clay Miner.* **2015**, 63, 432– 442 DOI: 10.1346/CCMN.2015.0630602

26. Van Olphen, H.; Fripiat, J. *Data Handbook for Clay Materials and Other Non-metallic Minerals*; Pergamon:Oxford, U.K., **1979**.

27. Moore, D. M.; Reynolds, R. C. *X-ray Diffraction and the Identification and Analysis of Clay Minerals*; Oxford University: Oxford, U.K., **1997**.

28. Müllejans, H.; French, R. H. Insights into the Electronic Structure of Ceramics through Quantitative Analysis of Valence Electron Energy-loss Spectroscopy *Microsc. Microanal.* **2000**, 6, 297– 306

29. Egerton, R. F. *Electron Energy-Loss Spectroscopy in the Electron Microscope*; Plenum: New York, **1996**.

30. Greene-Kelly, R. Birefringence of Clay Mineral Complexes *Clays Clay Miner.* **1961**, 10, 469– 475 DOI: 10.1346/CCMN.1961.0100141

31. Lifshitz, E. The Theory of Molecular Attractive Forces between Solids *Sov. Phys. JETP.* **1956**, 2, 73– 83

32. Dryden, D. M.; Hopkins, J. C.; Denoyer, L. K.; Poudel, L.; Steinmetz, N. F.; Ching, W.-Y.; Podgornik, R.; Parsegian, A.; French, R. H. van der Waals Interactions on the Mesoscale: Open-Science Implementation, Anisotropy, Retardation, and Solvent Effects *Langmuir* **2015**, 31, 10145– 10153 DOI: 10.1021/acs.langmuir.5b00106

33. Pignon, F.; Magnin, A.; Piau, J. M.; Cabane, B.; Lindner, P.; Diat, O. Yield stress thixotropic clay suspension: Investigations of structure by light, neutron, and x-ray scattering *Phys. Rev. E: Stat. Phys., Plasmas, Fluids, Relat. Interdiscip. Top.* **1997**, 56, 3281– 3289 DOI: 10.1103/PhysRevE.56.3281

34. Ganley, W. J.; van Duijneveldt, J. S. Controlling Clusters of Colloidal Platelets: Effects of Edge and Face Surface Chemistries on the Behavior of Montmorillonite Suspensions *Langmuir* **2015**, 31, 4377– 4385 DOI: 10.1021/acs.langmuir.5b00047

35. Segad, M.; Jönsson, B.; Cabane, B. Tactoid Formation in Montmorillonite *J. Phys. Chem. C* **2012**, 116,25425– 25433 DOI: 10.1021/jp3094929

36. Ramsay, J. D. F.; Swanton, S. W.; Bunce, J. Swelling and dispersion of smectite clay colloids: Determination of structure by neutron diffraction and small-angle neutron scattering *J. Chem. Soc., Faraday Trans.* **1990**,86, 3919– 3926 DOI: 10.1039/ft9908603919

37. Paineau, E.; Bihannic, I.; Baravian, C.; Philippe, A.-M.; Davidson, P.; Levitz, P.; Funari, S. S.; Rochas, C.;Michot, L. J. Aqueous Suspensions of Natural Swelling Clay Minerals. 1. Structure and Electrostatic Interactions *Langmuir* **2011**, 27, 5562– 5573 DOI: 10.1021/la2001255

38. Slade, P.; Quirk, J.; Norrish, K. Crystalline swelling of smectite samples in concentrated NaCl solutions in relation to layer charge *Clays Clay Miner.* **1991**, 39, 234– 238 DOI: 10.1346/CCMN.1991.0390302

39. Viani, B. E.; Low, P. F.; Roth, C. B. Direct measurement of the relation between interlayer force and interlayer distance in the swelling of montmorillonite *J. Colloid Interface Sci.* **1983**, 96, 229– 244 DOI: 10.1016/0021-9797(83)90025-5

40. Christidis, G. E.; Blum, A. E.; Eberl, D. D. Influence of layer charge and charge distribution of smectites on the flow behaviour and swelling of bentonites *Appl. Clay Sci.* **2006**, 34, 125– 138 DOI: 10.1016/j.clay.2006.05.008

41. Vao-soongnern, V.; Pipatpanukul, C.; Horpibulsuk, S. A combined X-ray absorption spectroscopy and molecular dynamic simulation to study the local structure potassium ion in hydrated montmorillonite *J. Mater. Sci.* **2015**, 50, 7126– 7136 DOI: 10.1007/s10853-015-9269-5

42. Salles, F.; Bildstein, O.; Douillard, J. M.; Jullien, M.; Van Damme, H. Determination of the Driving Force for the Hydration of the Swelling Clays from Computation of the Hydration Energy of the Interlayer Cations and the Clay Layer *J. Phys. Chem. C* **2007**, 111, 13170– 13176 DOI: 10.1021/jp0719762

43. Liu, X.; Lu, X. A thermodynamic understanding of clay swelling inhibition of interlayer potassium ion *Angew. Chem., Int. Ed.* **2006**, 45, 6300– 6303 DOI: 10.1002/anie.200601740

44. Zhang, Z.; Low, P. Relation between the heat of immersion and the initial water content of Li-, Na-, and K-montmorillonite *J. Colloid Interface Sci.* **1989**, 133, 461– 472 DOI: 10.1016/S0021-9797(89)80057-8

45. Anderson, R.; Ratcliffe, I.; Greenwell, H.; Williams, P.; Cliffe, S.; Coveney, P. Clay swelling — A challenge in the oilfield *Earth-Sci. Rev.* **2010**, 98, 201– 216 DOI: 10.1016/j.earscirev.2009.11.003

46. Bérend, I.; Cases, J.-M.; François, M.; Uriot, J.-P.; Michot, L.; Masion, A.; Thomas, F. Mechanism of adsorption and desorption of water vapor by homoionic montmorillonites: 2. The Li^+, Na^+, K^+, Rb^+, and Cs^+-exchanged forms *Clays Clay Miner.* **1995**, 43, 324– 336 DOI: 10.1346/CCMN.1995.0430307

47. Ferrage, E.; Lanson, B.; Sakharov, B. A.; Drits, V. A. Investigation of smectite hydration properties by modeling experimental X-ray diffraction patterns: Part I. Montmorillonite hydration properties *Am. Mineral.***2005**, 90, 1358– 1374 DOI: 10.2138/am.2005.1776

48. Li, H.; Peng, X.; Wu, L.; Jia, M.; Zhu, H. Surface Potential Dependence of the Hamaker Constant *J. Phys. Chem. C* **2009**, 113, 4419– 4426 DOI: 10.1021/jp808372r

49. Novich, B.; Ring, T. Colloid stability of clays using photon correlation spectroscopy *Clays Clay Miner.* **1984**,32, 400– 406 DOI: 10.1346/CCMN.1984.0320508

50. French, R. H.; Parsegian, V. A.; Podgornik, R.; Rajter, R. F.; Jagota, A.; Luo, J.; Asthagiri, D.;Chaudhury, M. K.; Chiang, Y.-M.; Granick, S.; Kalinin, S.; Kardar, M.; Kjellander, R.; Langreth, D. C.; Lewis, J.; Lustig, S.; Wesolowski, D.; Wettlaufer, J. S.; Ching, W.-Y.; Finnis, M.; Houlihan, F.; von Lilienfeld, O. A.; van Oss, C. J.; Zemb, T. Long range interactions in nanoscale science *Rev. Mod. Phys.***2010**, 82, 1887– 1944 DOI: 10.1103/RevModPhys.82.1887

51. Ambrosetti, A.; Ferri, N.; DiStasio, R. A., Jr.; Tkatchenko, A. Wavelike charge density fluctuations and van der Waals interactions at the nanoscale *Science* **2016**, 351, 1171– 1176 DOI: 10.1126/science.aae0509